Available online at www.sciencedirect.com
ScienceDirect
Journal of Power Sources 169 (2007) 35–39
JOURNAL OF POWER SOURCES
www.elsevier.com/locate/jpowsour

Short communication

Structural and electrical properties of thin films of $Pr_{0.8}Sr_{0.2}Fe_{0.8}Ni_{0.2}O_{3-\delta}$ ☆

I. Ruiz de Larramendi [a], R. López Antón [a], J.I. Ruiz de Larramendi [a], S. Baliteau [b], F. Mauvy [b], J.C. Grenier [b], T. Rojo [a,*]

[a] *Departamento de Química Inorgánica, Facultad de Ciencia y Tecnología, Universidad del País Vasco, Apdo.644, 48080 Bilbao, Spain*
[b] *Institut de Chimie de la Matière Condensée de Bordeaux I.C.M.C.B., C.N.R.S., 87 Avenue du Docteur Schweitzer 33608, Pessac Cedex, France*

Available online 6 February 2007

Abstract

$Pr_{0.8}Sr_{0.2}Fe_{0.8}Ni_{0.2}O_{3-\delta}$ (PN22) films have been deposited at different temperatures on yttria-stabilized zirconia (YSZ) substrates by pulsed laser deposition (PLD) for application to thin film solid oxide fuel cell cathodes. The structure of the films was analysed by X-ray diffraction (XRD) and atomic force microscopy (AFM). A marked influence in the structural properties of the substrate temperature has been found but not of the composition. Samples deposited at temperatures below 700 °C are amorphous, with granular aspect, and with decreasing roughness with the temperature. Meanwhile, the films at 700 °C are polycrystalline and exhibit a needle-shaped surface, with the highest roughness observed. Additionally, the conducting behaviour of the films has been studied by electrochemical impedance spectroscopy (EIS) and their cathodic area specific resistance (ASR) was determined. The main part of the impedance of the testing cells is due to the electrode. The ASR values of the films of PN22 are lower than those of $Pr_{0.9}Sr_{0.1}Fe_{0.8}Ni_{0.2}O_{3-\delta}$ (PN12), being the lowest 0.5 Ω cm^2 at 850 °C for the sample PN22 deposited at room temperature.

Keywords: SOFC; Cathodes; Perovskite; Pulsed laser deposition; Electrochemical impedance spectroscopy

1. Introduction

Solid oxide fuel cells (SOFC) are regarded as a feasible technology for generating electricity from hydrogen or hydrocarbon fuels. The most common materials for the SOFC are oxide ion conducting yttria-stabilized zirconia (YSZ) for the electrolyte, strontium-doped lanthanum manganite (LSM) for the cathode, nickel/YSZ for the anode and doped lanthanum chromite or refractory metals for the interconnect. Perovskite ferrites exhibit a variety of magnetic and electronic properties. Some of them display good performance as cathode materials in high temperature solid oxide fuel cells, because of their mixed, electronic and ionic conductivity. In particular, $Pr_{0.8}Sr_{0.2}Fe_{0.8}Ni_{0.2}O_{3-\delta}$ samples (PN22 in the following) present low electrical resistivity and they are also oxygen ion conductors [1]. On the other hand, pulsed laser deposition (PLD) has been recently used to fabricate La–Sr–Co–O thin films for application to SOFC [2–9], as using integrated oxide thin films for fuel cell design can reduce the size and cost of cells. Due to its high chemical reactivity with yttria-stabilized zirconia at high temperature [10], doped lanthanum cobaltite cannot be used as a cathode in high temperature SOFCs. Another important factor is the porosity in such a cathode, as it could help increase gas transport to the reaction sites at the surface of the electrolyte (usually yttria-stabilized zirconia, YSZ). Therefore, we have obtained several $Pr_{0.8}Sr_{0.2}Fe_{0.8}Ni_{0.2}O_3$ (PN22) thin films by PLD and studied the influence of the substrate temperature on the crystallinity and porosity of the samples, looking for thin films with high crystallinity and porosity. X-ray diffraction (XRD), atomic force microscopy (AFM) and electrical conductivity measurements have been performed so as to characterise them; results will be compare to those obtained with thin films of the $Pr_{0.9}Sr_{0.1}Fe_{0.8}Ni_{0.2}O_{3-\delta}$, PN12, phase, previously prepared [13].

☆ This paper presented at the 2nd National Congress on Fuel Cells, CONAPPICE 2006.

* Corresponding author. Tel.: +34 94 6012458; fax: +34 94 6013500.
E-mail address: teo.rojo@ehu.es (T. Rojo).

0378-7753/$ – see front matter © 2007 Elsevier B.V. All rights reserved.
doi:10.1016/j.jpowsour.2007.01.077

2. Experimental

Powders of $Pr_{0.8}Sr_{0.2}Fe_{0.8}Ni_{0.2}O_{3-\delta}$ were prepared according to combustion synthesis route using glycine as fuel. Appropriate amounts of the nitrate salts [$Pr(NO_3)_3{\cdot}5H_2O$; $Sr(NO_3)_2$; $Fe(NO_3)_3{\cdot}9H_2O$; $Ni(NO_3)_2{\cdot}6H_2O$] salts were dissolved in distilled water and glycine was later added to the solution. A concentrated gel was formed when the solution was dried and the nitrate-glycine-mixture-gel turns to a vigorous fire, which lasted until the combustion process was completed. The resulting powders were calcined first at 600 °C for 10 h in air, then pressed into pellets and calcined again at 1200 °C for 10 h.

Using these sintered pellets as targets, PSFNO films have been deposited on single crystal (1 0 0) YSZ substrates by PLD. The samples were deposited using a LAMBDA PHYSIC Compex 102 KrF excimer laser (248 nm, 150 mJ pulse^{-1}) at a frequency of 15 Hz. The target was placed in a rotating target holder in a vacuum chamber with an initial pressure of 2×10^{-6} mbar. The substrates were mounted on a heater and three films were deposited at different substrate temperatures: 20 °C (room temperature), 500 and 700 °C taking into account the existing literature [2–5] and our previous experience in PLD [11]. Oxygen gas was flowed into the chamber in a constant flux during deposition, keeping a pressure of 0.3 mbar. Deposition time was 120 min. An additional thin film was deposited at room temperature and annealed ex situ at 700 °C for 2 h in order to check whether an ex situ annealing was more adequate than growing the film at high temperature or not.

The powders and films were characterised by X-ray powder diffraction data, collected using a Philips PW1710 and Philips X'Pert-MPD (Bragg-Brentano geometry) diffractometers, with Cu Kα radiation, and fitted using the FULLPROF program [12]. The atomic force microscopy (AFM) measurements were performed using a commercial scanning probe microscope (Nanotec DSP classic).

Testing cells of PN22/YSZ/PN22 were made by deposition of $Pr_{0.8}Sr_{0.2}Fe_{0.8}Ni_{0.2}O_{3-\delta}$ on the two (polished) sides of a YSZ wafer, in order to measure their transport properties by electrochemical impedance spectroscopy (EIS) and to compare their properties with the already prepared cells of PN12/YSZ/PN12 [13]. The thickness of the substrate was $e \approx 0.50$ mm, whereas that of the films was about 3 μm, and the surface area, S roughly 0.55 cm^2. Electrical contacts were platinum grids pressed on both sides of the sample in order to obtain a symmetrical cell. In Fig. 1, a schematic drawing of the symmetrical testing cell is shown.

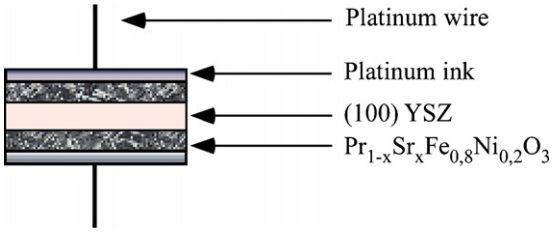

Fig. 1. Schematic drawing of the symmetrical testing cell.

Complex impedance spectroscopy measurements were carried out using an Autolab PGSTAT 30 Frequency Response Analyzer. The frequency range was 10^{-2} to 10^6 Hz with a signal amplitude of 50 mV. All these electrochemical experiments were performed at equilibrium from 800 °C down to 400 °C, i.e. under zero dc current intensity and under air over a cycle of heating and cooling. Impedance diagrams were analysed and fitted using the Zview software. Resistance, capacitance and self-values of equivalent circuits were thus obtained by least square refinement.

3. Results and discussion

The XRD diffractograms of the as-deposited thin films are shown in Fig. 2 whereas in Fig. 3 are shown the diffraction profile of the target and the fitted profiles of the thin film deposited at 700 °C (where the reflections due to the substrate have been eliminated) and of the film deposited at room temperature and then annealed at 700 °C. Very strong peaks due to the single crystal YSZ substrate are found in the as-deposited samples, as, e.g. the intense peak appearing at about 35 °C, corresponding to the (2 0 0) reflection of the substrate. In fact, this peak is so intense given the crystallinity of the substrate that even its corresponding Cu Kβ reflection is observed (despite the existence of a monochromator). No reflection due to the PN22 phase is found for the films deposited at temperatures lower than 700 °C, indicating their amorphous state. This is reasonable, given the complicated stoichiometry of the phase and the low temperatures of deposition, not allowing enough mobility to the atoms arriving at the substrate from the plume, so they become immobilised where they land (ballistic deposition). However, depositing at 700 °C, the atoms have enough mobility to reach the positions corresponding to the crystalline structure of the target and, therefore, the reflections corresponding to the PN22 crystalline phase are observed. It is noteworthy that, although the deposition conditions are adequate for an epitaxial growth, what we have is a polycrystalline film, due to the large discrepancy between the structures of YSZ (fluorite-type,

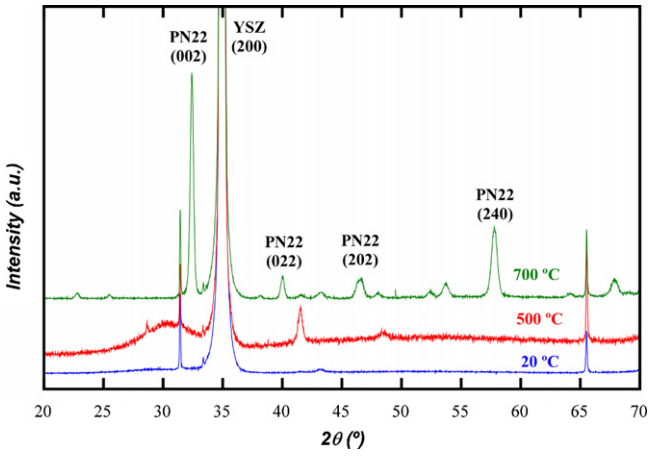

Fig. 2. XRD patterns of $Pr_{0.8}Sr_{0.2}Fe_{0.8}Ni_{0.2}O_{3-\delta}$ films obtained at room temperature, 500 and 700 °C.

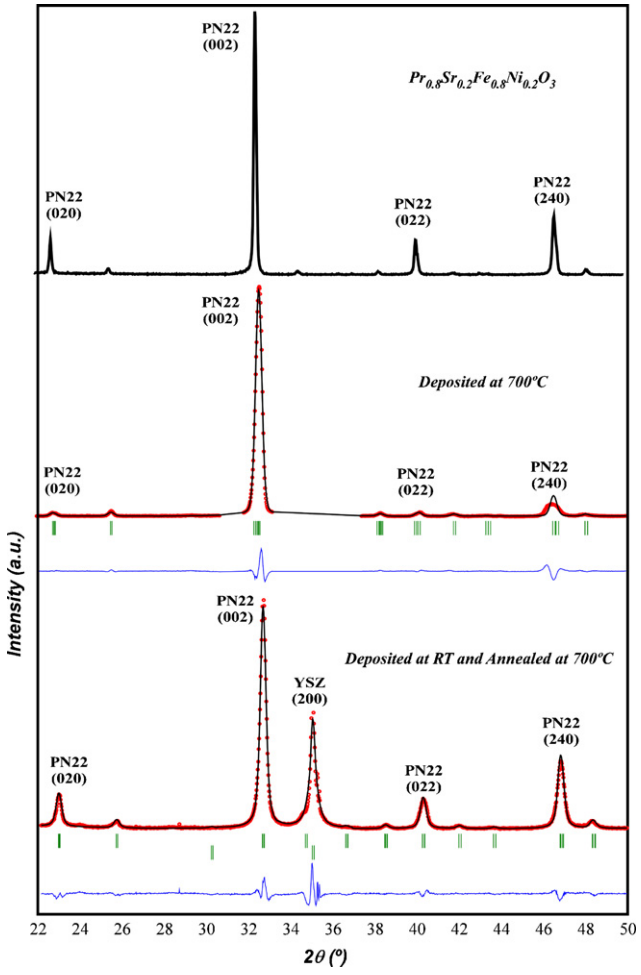

Fig. 3. Diffraction profiles of the PN22 phase: of the target (upper side) and experimental (squares), fitted (line) and difference between them (lower line) profiles of the thin film deposited at 700 °C (middle side) and deposited at room temperature and annealed at 700 °C (lower side).

*Fm*3*m* S.G.) and that of the target (perovskite-type *Pbnm* S.G.) [14]. Hence, we have a certain texture but not an epitaxial film (Fig. 2). Additionally, the partial oxygen pressure cannot only affect the oxygen stoichiometry but also the texture and orientation of this kind of films [4]. The peaks of the film are quite wider than those of the bulk, pointing out a smaller particle size and likely a certain stress in the film due to the commented structural difference between the substrate and the film.

Meanwhile, the sample deposited at room temperature and annealed 2 h in air at 700 °C also exhibits the reflections corresponding to the PN22 crystalline phase but lacking the texture observed in the film deposited at 700 °C (see Fig. 3), which can be easily understood given the different conditions of growth (ballistic deposition in one case, almost adequate for epitaxial growth in the other one).

The AFM micrographs of the films are shown in Fig. 4. It is observed that the topography changes strongly with the substrate temperature (in a similar way to the behaviour found in the PN12 phase [13]). In particular, the sample deposited at room temperature is quite rough, with a RMS roughness of 12.4 nm and a granular aspect, showing with clusters of about half a micron (Fig. 4a). This, together with the observed lack of crystallinity, agrees within a frame of a ballistic deposition.

The sample deposited at 500 °C exhibits a similar aspect but with a smoother surface (Fig. 4b). Hence, its RMS roughness is about 3 nm and the size of the clusters is smaller than in the previous sample. This can be understood given the higher mobility of the atoms and ions at the surface due to the higher temperature. However, the XRD measurements evidence the amorphousness of the sample, pinpointing that this increased mobility is not enough for reaching the crystalline state.

Meanwhile, the sample deposited at 700 °C shows a completely different aspect (Fig. 4c). Not only a sharp increase of the roughness is observed (RMS roughness of 35 nm) but also the topography changes drastically from that observed in the other films. In particular, the grains found are elongated, needle-shaped (with a long axis of about 0.8 μm and a short one of about 0.2 μm). These grains form clusters of a few grains with the same orientation as can be observed in the image. Noteworthily, at this temperature, the crystalline order also appears, so it seems that the topographic change is linked to the appearance of the ordered phase, likely due to the so different structures of the substrate and the film. However, it should be underlined that neither such a dramatic change in the topography with the temperature nor the needle-shaped topography are typical for these kinds of films [3,7].

In the case of the sample deposited at room temperature and annealed ex situ at 700 °C (Fig. 4d), it shows a granular aspect, as the original film, but with bigger agglomerates and with pores and cracks of increased size, which agrees well with the results found by Chen et al. for the La–Sr–Co–O system [3]. Its RMS roughness, of about 32 nm, is fairly similar to that of the sample deposited at 700 °C but, however, no needle-shaped structures are found. According to the XRD measurements, the sample shows the same crystalline phase as the target but lacking the texture observed in the film deposited at 700 °C. Therefore, these needle-shaped structures are linked to the deposition conditions and not only to the crystalline order.

Typical electrochemical impedance spectra for PN12/YSZ/PN12 cells are reported in the Nyquist plan at 335 °C (Fig. 5) and at 800 °C (Fig. 6). Meanwhile, in Fig. 7, Nyquist plots of PN22/YSZ/PN22 cell measured at various temperatures, in air, are shown. In all cases, no grain boundary contribution of the electrolyte is found as it is a single crystal. At low temperatures, the semicircles due to the electrolyte are observed whereas at high temperature the phenomena characterising the cathode (interface processes, electrode reactions, . . .) are found. The oxygen reduction mechanism on porous MIEC (mixed ionic and electronic conductors) electrodes may involve several processes, such as charge transfer at the current collector/electrode interface and electrode/electrolyte interfaces, oxygen exchange at the electrode surface, bulk and surface diffusion of oxygen species and gas phase diffusion.

At 335 °C, the impedance spectrum is characterised by two depressed semicircles at high and low frequencies (HF and LF, respectively). Concerning the HF contribution, the mean value of the capacitive effect is around 5×10^{-11} F, value which is usually found for the YSZ bulk response according to literature

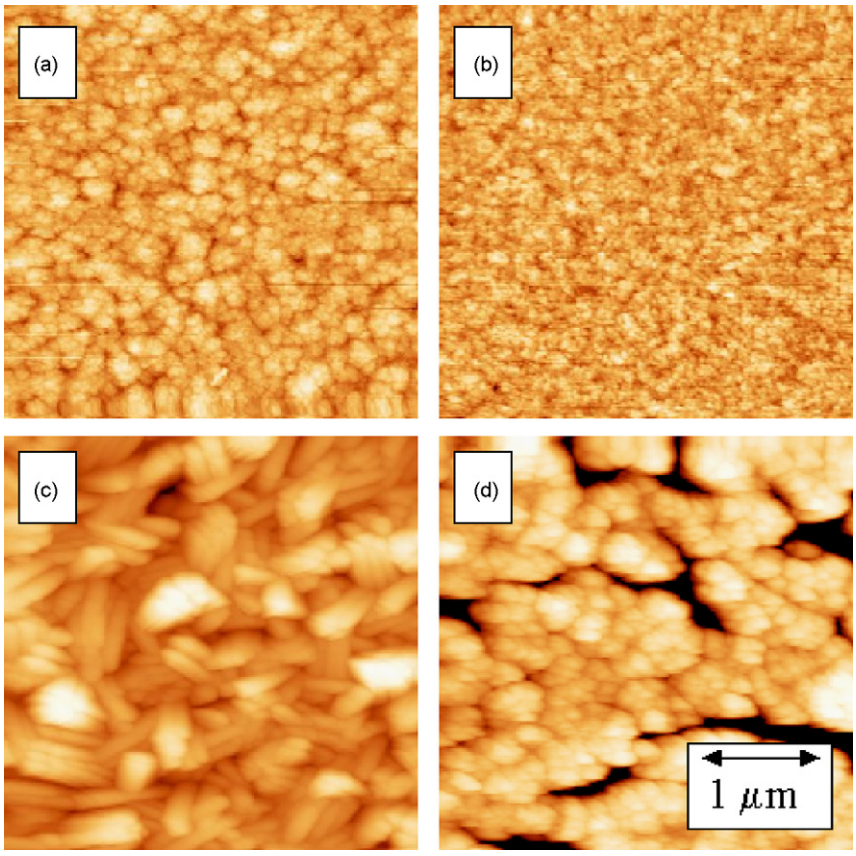

Fig. 4. AFM micrographs of the films deposited at different temperatures: (a) room temperature, (b) 500 °C and (c) 700 °C; (d) deposited at room temperature and then annealed at 700 °C for 2 h. The frame size of the images is 3.5 μm × 3.5 μm.

[15–16]. The second semicircle, corresponding to the LF contribution, is assigned to the air electrode processes. At higher temperatures, the electrode impedance becomes more important than bulk contribution (see Figs. 6 and 7). The high frequency part represents the bulk impedance (R_{YSZ}) associated to the inductive contribution of the platinum wires used as current collectors. Low frequency contributions can also be associated to the electrode processes. According to this identification, the electrode resistance $R_{electrode}$ is obtained by the difference of the intercepts of the LF asymmetric arc with the real axis [17].

Then, the cathodic area specific resistance (ASR) is deduced from the relation: ASR = $R_{electrode}$ × surface/2. The Arrhenius plots of the ASRs for PN12/YSZ and PN22/YSZ half cells are given in Fig. 8.

Concerning the PN12 series, at 850 °C, the ASRs remain higher than 1 Ω cm^2 for all the samples, whatever the deposition process, the lowest one being that of the RT deposit. For the PN22 series, the sample deposited at room temperature again shows the lowest ASR value (≈0.5 Ω cm^2 at 850 °C). This is

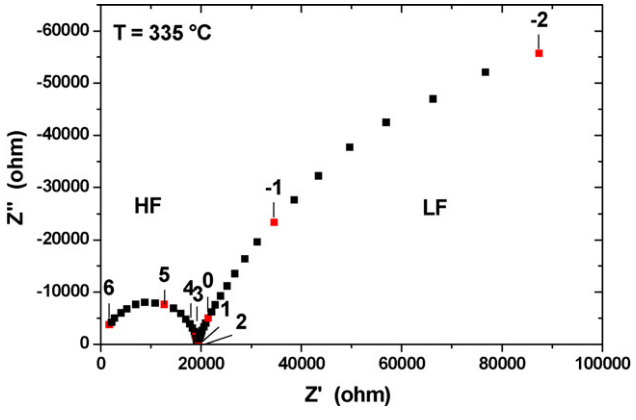

Fig. 5. Typical impedance diagrams obtained with PN12/YSZ half cells, under air, at 335 °C. The numbers indicate the frequency logarithm.

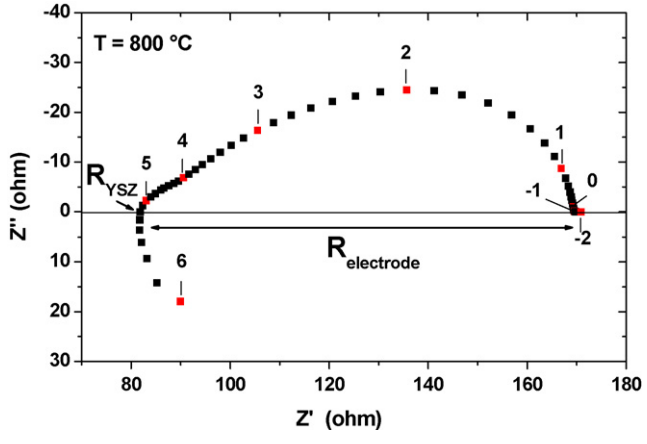

Fig. 6. Typical impedance diagrams obtained with PN12/YSZ half cells, under air, at 800 °C. The numbers indicate the frequency logarithm.

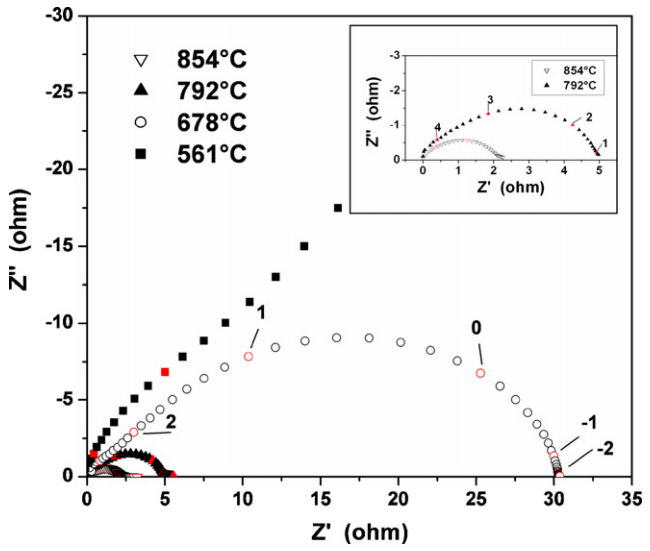

Fig. 7. Typical Nyquist plots of PN22/YSZ/PN22 cell measured at various temperatures, in air. The impedance data are plotted after electrolyte ohmic drop correction. The numbers by data points are frequency logarithms. *Inset*: Detail of the plots obtained at high temperatures.

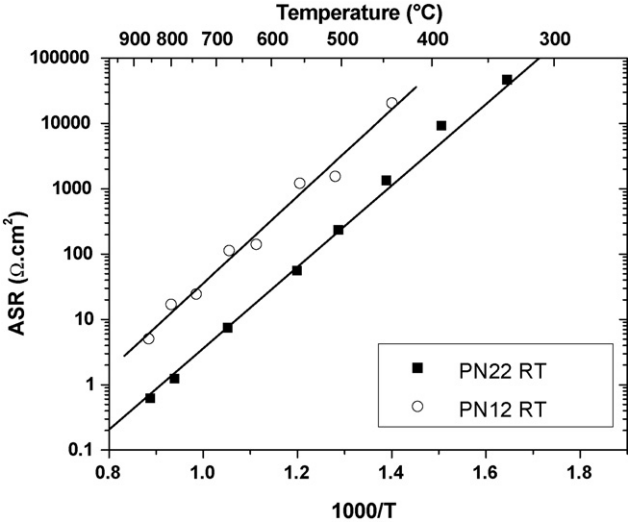

Fig. 8. Arrhenius plots of the ASRs for PN12/YSZ and PN22/YSZ, deposited at room temperature.

likely assigned to the high porosity of the samples deposited in such a way. Furthermore, from the Arrhenius plots, the value of the ASR activation energy is $E_A = 1.3$ eV, which is a value usually observed for electrode polarisation.

4. Conclusions

Polycrystalline thin films of $Pr_{0.8}Sr_{0.2}Fe_{0.8}Ni_{0.2}O_3$ have been deposited on YSZ substrates at different temperatures. The samples deposited at room temperature and at 500 °C are amorphous and with a granular aspect whereas the film deposited at 700 °C is a polycrystalline thin film, with certain texture, with needle-shaped topography which increased strongly the porosity, making them well suited for application to solid oxide fuel cell electrodes. Meanwhile, the sample deposited at room temperature and annealed at 700 °C is polycrystalline, without texture, and shows a granular aspect but with big agglomerates and with abundant pores and cracks, and without the needle-shaped structures, which is hence linked to the growth conditions. The main part of the impedance of the testing cells is due to the electrode. The ASR values of the films of $Pr_{0.8}Sr_{0.2}Fe_{0.8}Ni_{0.2}O_{3-\delta}$ are lower than those of $Pr_{0.9}Sr_{0.1}Fe_{0.8}Ni_{0.2}O_{3-\delta}$, the lowest one being 0.5 Ω cm^2, at 850 °C, for the film deposited at room temperature.

Acknowledgements

This work has been partially financed by the Spanish CiCyT under project MAT2004-02425. I. Ruiz de Larramendi thanks the Eusko Jaurlaritza/Gobierno Vasco for her predoctoral fellowship and R.L.A. thanks the Spanish CiCyT for funding his research activities as postdoc within the Project MAT2004-02425.

References

[1] S.-I. Hashimoto, K. Kammer, P.H. Larsen, F.W. Pulsen, M. Mogensen, Solid State Ionics 176 (2005) 1013–1020.
[2] X. Chen, N.J. Wu, A. Ignatiev, J. Eur. Ceram. Soc. 19 (1999) 819–822.
[3] X. Chen, N.J. Wu, D.L. Ritums, A. Ignatiev, Thin Solid Films 342 (1999) 61–66.
[4] X. Chen, S. Wang, Y.L. Yang, L. Smith, N.J. Wu, B.-I. Kim, S.S. Perry, A.J. Jacobson, A. Ignatiev, Solid State Ionics 146 (3, 4) (2002) 405–413.
[5] X. Chen, N.J. Wu, L. Smith, A. Ignatiev, Appl. Phys. Lett. 84 (2004) 2700–2702.
[6] N. Imanishi, T. Matsumura, Y. Sumiya, K. Yoshimura, A. Hirano, Y. Takeda, D. Mori, R. Kanno, Solid State Ionics 174 (2004) 245–252.
[7] D. Mori, H. Oka, Y. Suzuki, N. Sonoyama, A. Yamada, R. Kanno, Y. Sumiya, N. Imanishi, Y. Takeda, Solid State Ionics 177 (2006) 535–540.
[8] N. Imanishi, Y. Sumiya, K. Yoshimura, T. Matsumura, A. Hirano, Y. Takeda, D. Mori, R. Kanno, Solid State Ionics 177 (2006) 749–755.
[9] L.R. Pederson, P. Singh, X.-D. Zhou, Vacuum 80 (2006) 1066–1083.
[10] F.M. Figueiredo, J.A. Labrincha, J.R. Frade, F.M.B. Marques, Solid State Ionics 101 (1997) 343.
[11] R. López Anton, J.J. Blanco, J.L. Muñoz, J.S. Garitaonandia, M. Insausti, A. Peña, T. Rojo, M.L. Fdez-Gubieda, J.M. Barandiarán, Mater. Sci. Forum 373-376 (2001) 577–580;
R. Lopez Anton, Ph.D. Thesis, Univ. País Vasco, 2002.
[12] J. Rodríguez-Carvajal, FULLPROF Program, ILL, Grenoble, 1994.
[13] I. Ruiz de Larramendi, R. López Antón, J.I. Ruiz de Larramendi, F. Mauvy, M.I. Arriortua, J.C. Grenier, T. Rojo, Seventh European Solid Oxide Fuel Cell Forum, Lucerne (Switzerland), 2006, p. P0609.
[14] M. Esteve, F. Castaño, F.J. Castaño, B. Vögeli, J. Non-Cryst. Solids 287 (1–3) (2001) 1–4.
[15] E.J.L. Schouler, N. Mesbahi, G. Vitter, Solid State Ionics 9 and 10 (1993) 989–996.
[16] J.B. Goodenough, Solid State Ionics 97 (1997) 17–25.
[17] C. Lalanne, F. Mauvy, J.-M. Bassat, J.C. Grenier, P. Dordor, M. Pouchard, P. Stevens, in: M. Mogensen (Ed.), Sixth European Solid Oxide Fuel Cell Forum, Oberrohrdorf (Switzerland), 2004, pp. 1351–1358.